1-1-2015

A Cu_4S Model for the Nitrous Oxide Reductase Active Sites Supported Only by Nitrogen Ligands

Brittany J. Johnson
University of Illinois at Chicago

William E. Antholine
Medical College of Wisconsin

Sergey V. Lindeman
Marquette University, sergey.lindeman@marquette.edu

Neal P. Mankad
University of Illinois at Chicago

Accepted version. *Chemical Communications,* Vol. 51 (2015): 11860-11863. DOI.

A Cu_4S Model for the Nitrous Oxide Reductase Active Sites Supported Only by Nitrogen Ligands

Brittany J. Johnson
Department of Chemistry, University of Illinois at Chicago, Chicago, IL
William E. Antholine
Department of Biophysics, Medical College of Wisconsin, Milwaukee, WI
Sergey V. Lindeman
Department of Chemistry, Marquette University, Milwaukee, WI
Neal P. Mankad
Department of Chemistry, University of Illinois at Chicago, Chicago, IL

Abstract: To model the $(His)_7Cu_4S_n$ (n = 1 or 2) active sites of nitrous oxide reductase, the first $Cu_4(\mu_4\text{-}S)$ cluster supported only by nitrogen donors has been prepared using amidinate supporting ligands. Structural, magnetic, spectroscopic, and computational characterization is reported. Electrochemical

Chemical Communications, Vol 51 (2015): pg. 11860-11863. DOI.

data indicates that the 2-hole model complex can be reduced reversibly to the 1-hole state and irreversibly to the fully reduced state.

Nitrous oxide reductase (N_2OR) is a copper-dependent enzyme that converts environmentally harmful nitrous oxide into benign dinitrogen and water during bacterial denitrification.[1] Two forms of the N_2O-reducing active site of N_2OR have been characterized crystallographically (Figure 1a). Both feature $Cu_4(\mu_4\text{-}S)$ cores supported by seven histidine *N*-donors; the Cu_Z* form features a hydroxide/water ligand along one edge of the tetracopper cluster,[2,3] while the Cu_Z form instead features a second sulphide ligand along that edge.[4] The Cu_Z* site has a "1-hole" $Cu^I_3Cu^{II}$ resting state and activates N_2O rapidly in the "fully reduced" Cu^I_4 state, while the Cu_Z site has a "2-hole" $Cu^I_2Cu^{II}_2$ resting state and activates N_2O slowly in its "1-hole" state.[5] The electronic structure descriptions and chemical mechanisms related to these active sites remain elusive, motivating model studies.

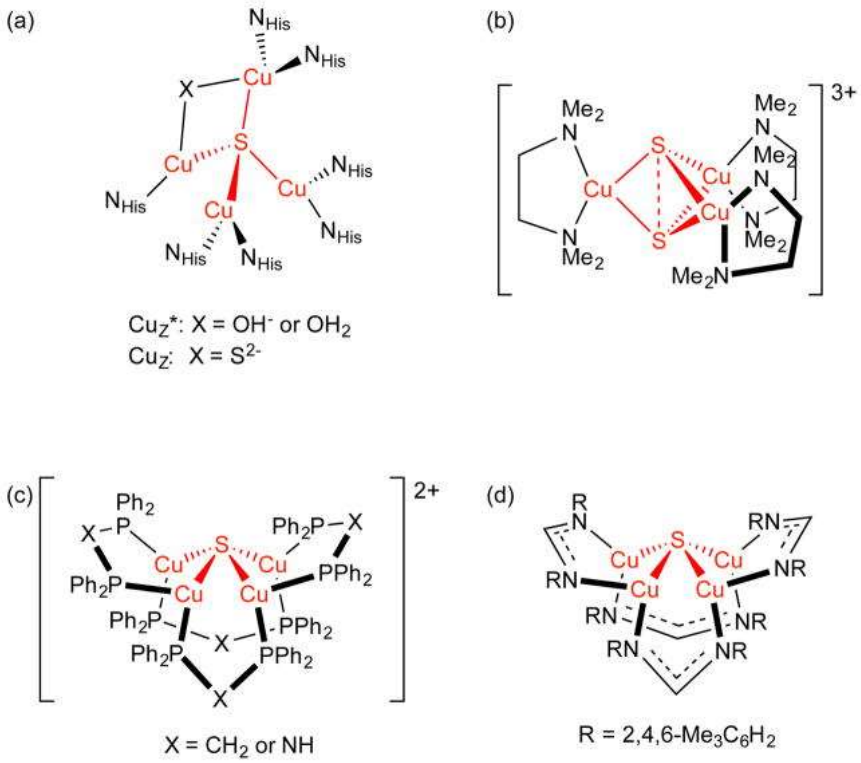

Figure 1. (a) Structures of the Cu_Z* and Cu_Z active sites of nitrous oxide reductase; (b) a representative Cu_3S_2 model complex with nitrogen ligands; (c) previously reported $Cu_4(\mu_4\text{-}S)$ model complexes with phosphorous ligands; (d) the $Cu_4(\mu_4\text{-}S)$ model complex reported in this work.

Chemical Communications, Vol 51 (2015): pg. 11860-11863. DOI.

Much of the available knowledge regarding copper sulphide clusters comes from studies of Cu_2S_2[6] and Cu_3S_2[7,8] model complexes, which feature bridging ligands with significant S-S interactions,[9] supported by nitrogen chelates. The latter category of complexes (Figure 1b), in particular, has been the subject of extensive experimental and computational characterization as well as fascinating literature discussions.[9–11] However, none of these complexes truly model the unusual μ_4-S bridge of N_2OR or provide insight into reduced catalytic intermediates. Phosphine[12,13] ligands have been used to stabilize "fully reduced" $Cu_4(\mu_4\text{-S})$ and $Cu_3(\mu_3\text{-S})$ clusters more structurally faithful to N_2OR (Figure 1c), but the inability thus far of these systems to access open-shell oxidation states has precluded experimental determination of electron structure using typical methods of physical inorganic chemistry.[14] In this regard, a recent report of strained $Cu_3(\mu_3\text{-S})$ clusters encapsulated within a tris(β-diketinimate) cyclophane cage was a noteworthy advance.[15] In this communication, we report the first $Cu_4(\mu_4\text{-S})$ cluster supported only by nitrogen ligands (Figure 1d) and disclose its structural, magnetic, and spectroscopic characterization. This system will provide an entry point for electronic structure determination and chemical reactivity studies for a tetracopper sulphide environment that is, arguably, the most relevant model for N_2OR identified to date.

Inspired by a recent study of copper amidinate clusters assembled using carbon disulphide,[16] we sought to study copper sulphide chemistry using the amidinate ligand, $[(2,4,6\text{-}Me_3C_6H_2N)_2CH]^-$ (abbreviated NCN^- here). Addition of the neutral sulphur atom donors S_8 or Ph_3SbS to the dicopper(I) precursor $(NCN)_2Cu_2$ resulted in a dramatic colour change from colourless to dark purple. While this purple product (**1**) formed in low yields due to its instability in solution as well as the formation of several side products, we were able to isolate **1** in yields of 34–43%. Elemental analysis data for this material was consistent with a $(NCN)_4Cu_4S$ stoichiometry, and this assignment was confirmed by single-crystal X-ray diffraction. Complex **1** crystallizes in the $P\bar{4}3n$ space group. The crystal symmetry coincides with the local symmetry of the NCN^- ligand shell, which is highly ordered about the crystallographic $\bar{4}$ through possible stabilization from π-stacking interactions (Figure 2). (This structure is apparently rigid in solution as evidenced by NMR spectroscopy, where six distinct mesityl methyl resonances were resolved, indicating

restricted N-C_{aryl} bond rotation as well as static pseudo-S_4 symmetry in solution that distinguishes the "upwards" NCN^- ligands from the "downwards" NCN^- ligands. See Figures S5, S6 and S16.) However, the crystal symmetry results in two alternative positions for the Cu_4S core that apparently has lower internal symmetry (Figure S15).

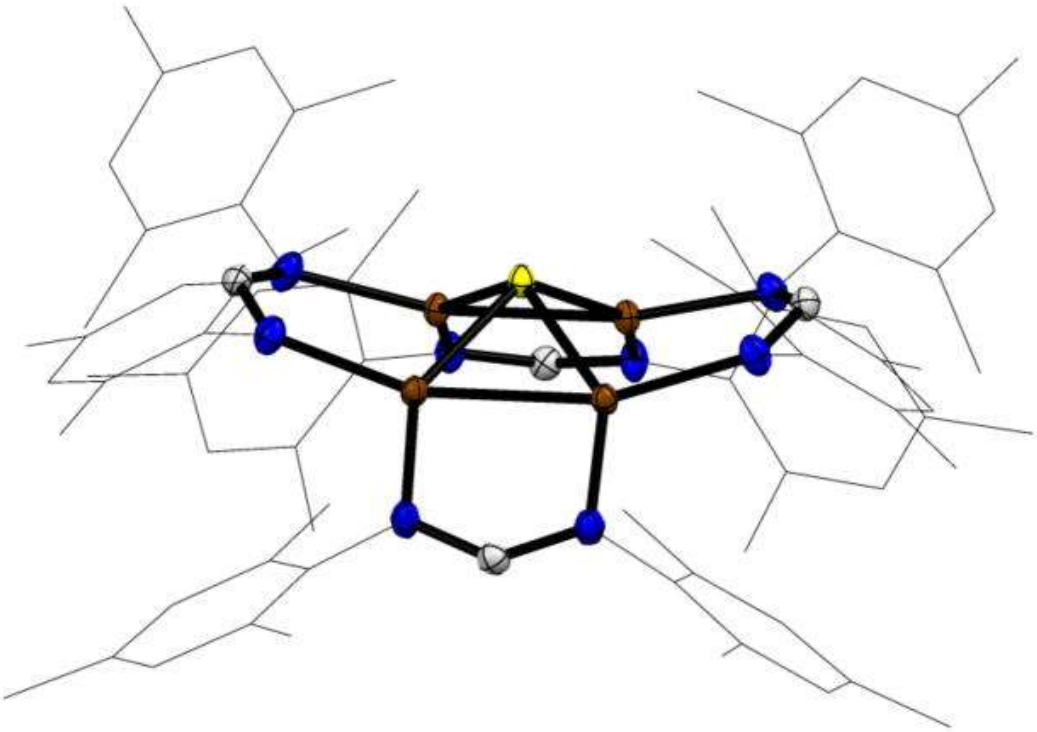

Figure 2. X-ray structure of **1**, with only one of two disordered Cu_4S components shown. Mesityl groups are shown as wireframes, other atoms are shown as 50%-probability thermal ellipsoids, and hydrogen atoms have been omitted. Colour scheme: C, grey; Cu, brown; N, blue; S, yellow.

The exact assignment of alternative Cu and S positions to one or another component of the crystallographic disorder was done by analysing Cu-Cu and Cu-S separations from the point of view of structurally meaningful values. This assignment was confirmed by DFT calculations. Spin-unrestricted and symmetry-unrestricted DFT calculations at the BVP86/LANL2TZ(f) level of theory were conducted for both singlet and triplet spin states using a model where the *N*-mesityl groups were changed to *N*-methyl groups (**1-Me**). The singlet state for **1-Me** was calculated to be lower in energy than the triplet state (by 10.2 kcal/mol, although more advanced calculations would be needed to accurately estimate the singlet-triplet gap). The

optimized structure of the singlet state has C_{2V} symmetry and is characterized by an alternating short-long-short-long pattern of Cu-Cu distances within the Cu_4 rectangle, with short Cu-Cu distances of 2.45 Å and long Cu-Cu distances of 2.79 Å. It is tempting, based on these bond distances, to view the **1-Me** structure as consisting of two separate $[Cu^{1.5}Cu^{1.5}]$ units that are antiferromagnetically coupled to each other, giving rise to the singlet ground state. However, the two optimized structures were found to have stable wavefunctions with respect to internal magnetic coupling, and the α and β molecular orbitals for the singlet state were degenerate and identical in nature. Collectively, these observations indicate that **1-Me** is best described at this time as having a closed-shell singlet ground state rather than a singlet state arising from magnetic coupling, at this level of theory.

Only one Cu_4S set can be identified from the disordered crystal structure of **1** that matches the topology and key structural features of optimized singlet **1-Me**. The resulting structure (Figure 2) for **1** possesses near-perfect C_{2V} symmetry and replicates the calculated bond length alternation in the Cu_4 rectangle of **1-Me**, with experimentally determined short Cu-Cu distances of 2.4226(6) Å and long Cu-Cu distances of 3.0353(6) Å. Within this component, the two sets of Cu-S distances are 2.1812(6) Å and 2.1790(6) Å. The geometry at sulphur is characterized by a τ_4 value[17] of 0.76, similar to the τ_4 values for the μ_4-S ligands in Cu_Z* (0.66) and Cu_Z (0.71).

The formal oxidation state assignment for **1** is $Cu^{I}_2Cu^{II}_2$, making it a model for the "2-hole" state of the N_2OR active site. The 2-hole Cu_Z is also a singlet ground state.[1] The purple colour of **1** comes from two overlapping absorbance peaks (Figure 3): a main peak centred at 561 nm ($\varepsilon \approx 14000\ M^{-1}cm^{-1}$) and a shoulder at approximately 470 nm. For comparison, the 2-hole Cu_Z absorbs at 540 nm and the 1-hole Cu_Z* absorbs at 680 nm.[5] To our knowledge, the 2-hole Cu_Z* has not been characterized.

Chemical Communications, Vol 51 (2015): pg. 11860-11863. DOI.

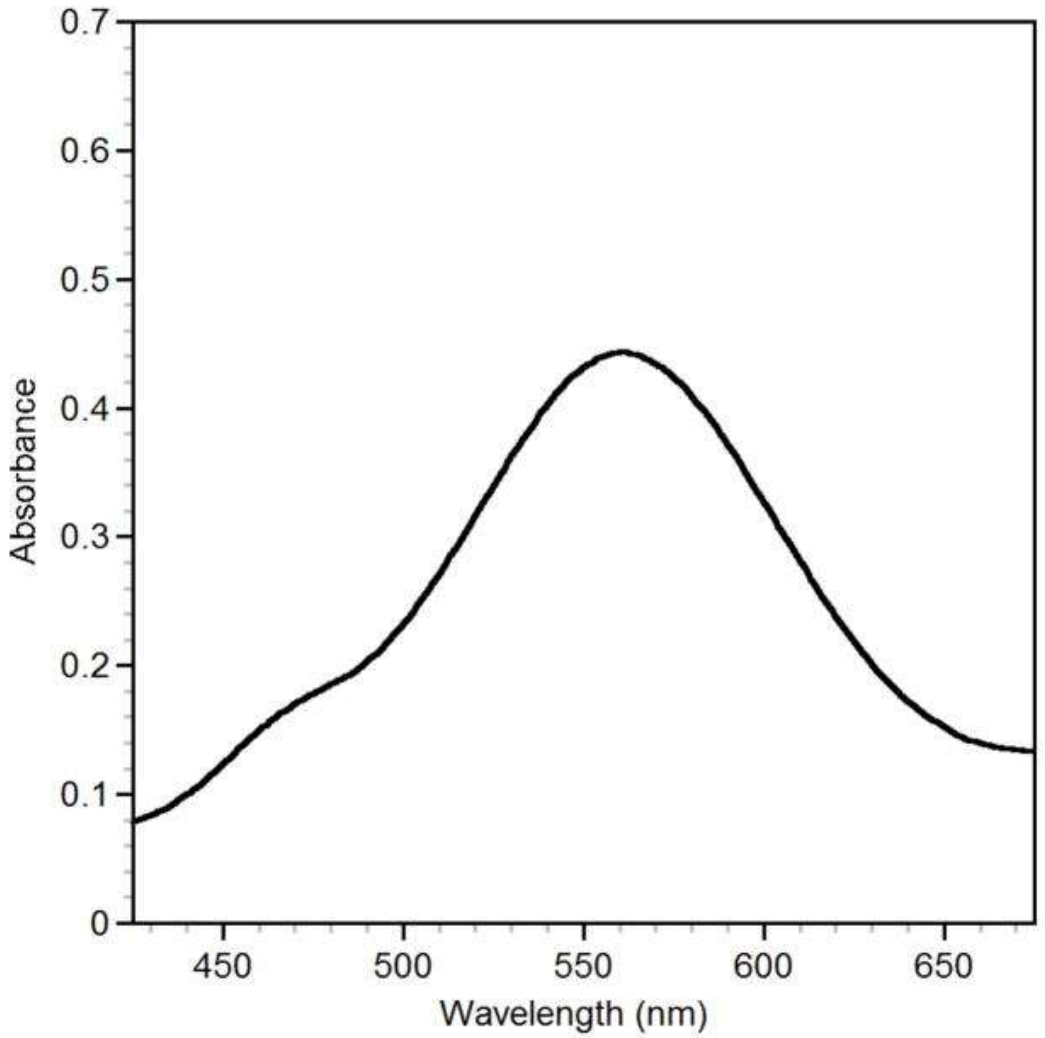

Figure 3. Absorbance spectrum of **1** (0.06 mM solution in CH_2Cl_2).

The accumulated experimental data is consistent with **1** possessing a singlet ground state with a low-energy triplet excited state. The ^{1}H and ^{13}C{^{1}H} NMR spectra for **1** resemble those for a typical diamagnetic species, with chemical shifts occurring in their normal regions. However, complex **1** exhibits a measurable magnetic moment in solution that increases with increasing temperature (μ_{eff} = 2.3–2.9 μ_B over the temperature range 221–298 K; see Figure S1). In addition, a frozen glass containing **1** was found to be EPR active. The observed EPR spectrum seems typical for a monomeric S = 1/2 cupric species with splitting from one Cu and two equivalent N centres ($g_{||}$ = 2.134, $A_{||}$(Cu) = 185 G, $A_{||}$(N) = 15 G; see Figure S18a–b). Notably, the intensity of the EPR signal was found to increase by a factor of 2.5

as the temperature was increased from 115 K to 130 K. Upon decreasing the temperature from 130 K to 112 K, the signal intensity decreased, indicating that the temperature dependence is reversible. For a typical S = 1/2 signal, the Curie Law predicts that the signal intensity should decrease by a factor of 115/130 = 0.88 when warmed from 115 K to 130 K, as we confirmed by analysing $Cu(acac)_2$ as an authentic S = 1/2 control sample (Figure S18c). The increase in signal intensity with increasing temperature could be a further indication that a paramagnetic excited state is being thermally populated. While it is not clear how the observed EPR signal fits the magnetic properties of **1**, the reversible temperature dependence is unusual. Even if after further studies the S = 1/2 turns out to derive from a trace paramagnetic byproduct or decomposition material, or even from a temperature-dependent comproportionation equilibrium, the magnetic properties for the S = 1/2 complex are novel and warrant further explanation, which is beyond the scope of this investigation. It is worth noting that there is precedent for dicopper sites with EPR spectra resembling monomeric cupric species.[18–21]

The cyclic voltammetry of **1** was examined in both CH_2Cl_2, which provides access to more oxidizing potentials, and THF, which provides access to more reducing potentials. In CH_2Cl_2 (Figure 4a), the cyclic voltammogram (CV) of **1** featured a reversible wave centred at −1.28 V vs Fc^+/Fc (Fc = ferrocene), which is assigned as the **1**/[**1**]$^-$ couple, as well as two quasi-reversible waves at +0.51 and approximately +0.92 V vs Fc^+/Fc. These oxidative events are assigned as ligand-based oxidations for two reasons. First, nearly identical signatures were found in the CV of the $(NCN)_2Cu_2$ precursor (Figure S11). Second, a closely related amidinate-supported dicopper system is known to engage in predominantly ligand-based redox chemistry at similar potentials.[22] In THF (Figure 4b), the **1**/[**1**]$^-$ couple was observed at −1.25 V vs Fc^+/Fc, and an additional irreversible reduction to [**1**]$^{2-}$ was observed with onset at approximately −2.36 V vs Fc^+/Fc. Collectively, the CV data indicates that (a) oxidation of **1** occurs from the NCN^- ligands, (b) the formally $Cu^I_3Cu^{II}$ "1-hole" species also is stabilized in this system, and (c) further ligand modification is needed to stabilize the formally Cu^I_4 "fully reduced" oxidation state that would model the active form of Cu_Z*.

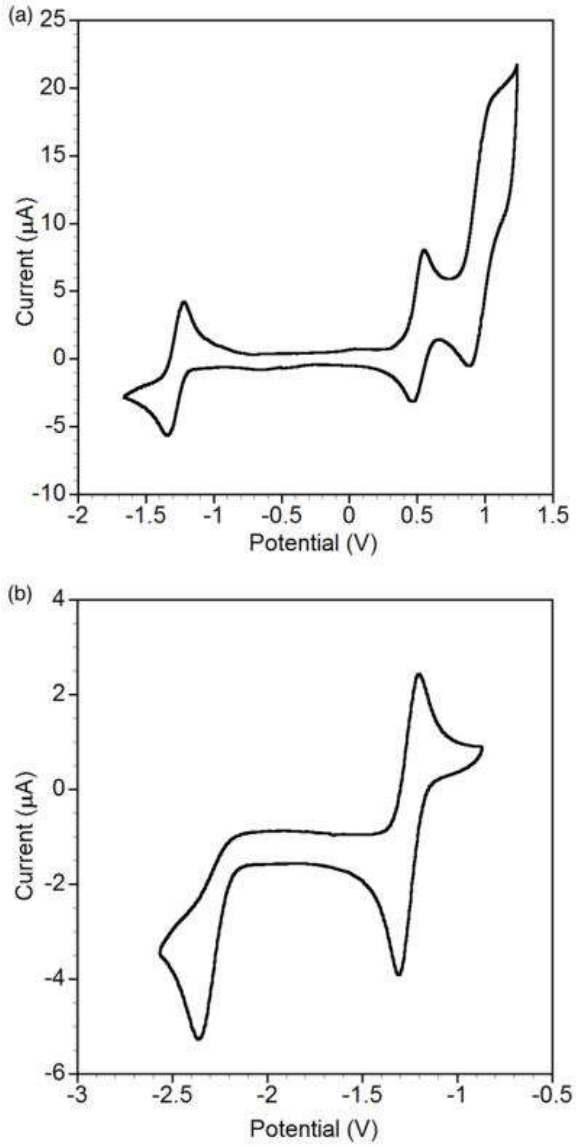

Figure 4. Cyclic voltammograms of **1** with 0.1 M $[NBu_4][PF_6]$ electrolyte in (a) CH_2Cl_2 and (b) THF.

Lastly, information about the frontier orbitals can be obtained from the calculated DFT structure of **1-Me** and is largely consistent with the collected experimental data. The calculated **1-Me** HOMO (Figure 5a), which models the source of electrons during oxidation of **1**, is mostly based on two of the NCN^- ligands, with MO populations of 60% total N 2*p* (15% each), 7% S 3*p*, and and 16% total Cu 3*d* (4% each). The calculated **1-Me** LUMO (Figure 5b), which models the destination of electrons during reduction of **1** to the 1-hole and fully reduced states, is mostly based on the covalent $Cu_4(\mu_4\text{-}S)$ core, with

MO populations of 21% S 3*p*, 48% total Cu 3*d* (12% each), and 12% total N 2*p* (3% each).

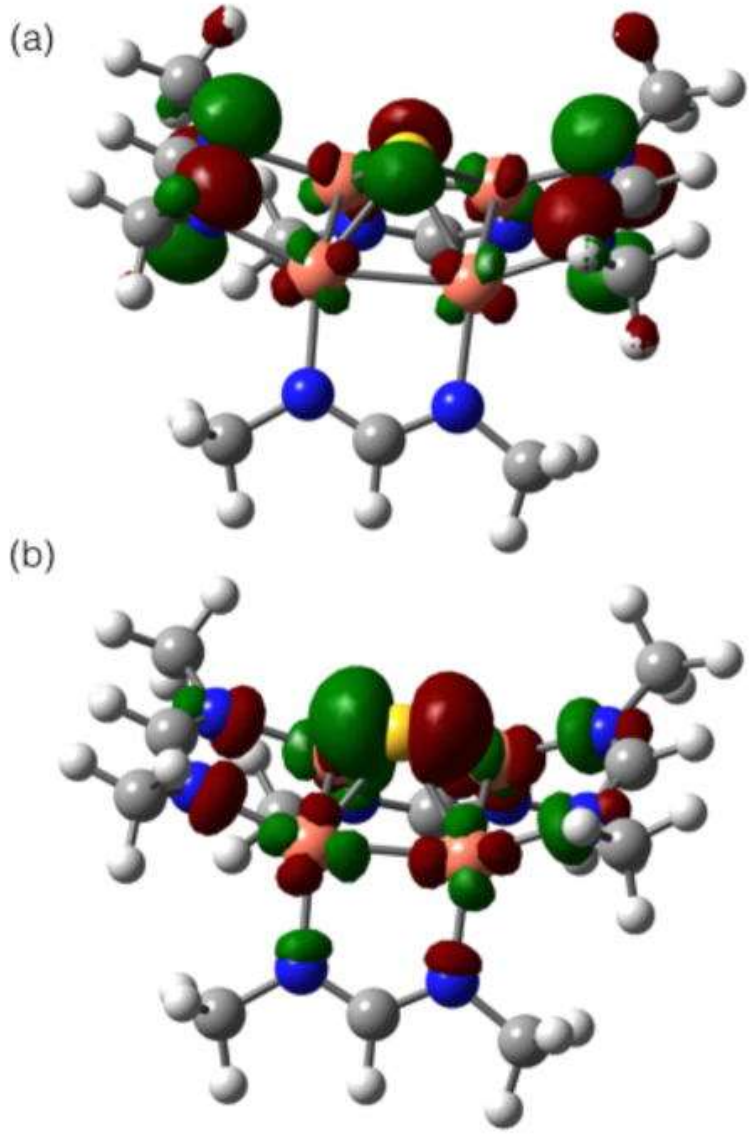

Figure 5. Calculated (a) HOMO and (b) LUMO for **1-Me** (0.04 isovalue).

In conclusion, this report discloses the synthesis and thorough characterization of copper sulphide cluster **1**, which represents the most relevant model for the active sites of N_2OR to date from the perspective of featuring a $Cu_4(\mu_4\text{-}S)$ core supported only by nitrogen ligands. While structurally similar to the Cu_Z* site, model **1** possesses redox chemistry reminiscent of the more electron-rich Cu_Z site, presumably due to the presence of anionic amidinate ligands in place

Chemical Communications, Vol 51 (2015): pg. 11860-11863. DOI.

of neutral histidine donors. On-going efforts in our laboratory involve accessing reduced oxidation states of **1** for more thorough electronic structure measurements and chemical reactivity studies.

Footnotes

†Start-up funds to N.P.M. were provided by the UIC Department of Chemistry. EPR facilities are supported by the National Biomedical EPR Center Grant EB001980 from NIH. The authors are grateful to members of the Mankad group for verifying reproducibility of the synthetic procedures.

Electronic Supplementary Information (ESI) available: Experimental and computational methods, spectral and crystallographic data, computational output. CCDC deposition number for **1**: CCDC 1405092. See DOI: 10.1039/x0xx00000x

Notes and references

[1]Pauleta SR, Dell'Acqua S, Moura I. *Coord Chem Rev.* 2013;257:332–349.
[2]Brown K, Tegoni M, Prudêncio M, Pereira AS, Besson S, Moura JJ, Moura I, Cambillau C. *Nat Struct Biol.* 2000;7:191–195.
[3]Rasmussen T, Berks BC, Sanders-Loehr J, Dooley DM, Zumft WG, Thomson AJ. *Biochemistry*. 2000;39:12753–12756.
[4]Pomowski A, Zumft WG, Kroneck PMH, Einsle O. *Nature*. 2011;477:234–237.
[5]Johnston EM, Dell'Acqua S, Ramos S, Pauleta SR, Moura I, Solomon EI. *J Am Chem Soc.* 2013;136:614–617.
[6]Sarangi R, York JT, Helton ME, Fujisawa K, Karlin KD, Tolman WB, Hodgson KO, Hedman B, Solomon EI. *J Am Chem Soc.* 2008;130:676–686.
[7]Brown EC, York JT, Antholine WE, Ruiz E, Alvarez S, Tolman WB. *J Am Chem Soc.* 2005;127:13752–13753.
[8]Bar-Nahum I, Gupta AK, Huber SM, Ertem MZ, Cramer CJ, Tolman WB. *J Am Chem Soc.* 2009;131:2812–2814.
[9]Sarangi R, Yang L, Winikoff SG, Gagliardi L, Cramer CJ, Tolman WB, Solomon EI. *J Am Chem Soc.* 2011;133:17180–17191.
[10]Berry JF. *Chem Eur J.* 2010;16:2719–2724.
[11]Alvarez S, Hoffmann R, Mealli C. *Chem Eur J.* 2009;15:8358–8373.
[12]Yam VWW, Lee WK, Lai TF. *J Chem Soc, Chem Commun.* 1993;1571
[13]Johnson BJ, Lindeman SV, Mankad NP. *Inorg Chem.* 2014;53:10611–10619.
[14]York JT, Bar-Nahum I, Tolman WB. *Inorg Chim Acta.* 2008;361:885–893.
[15]Di Francesco GN, Gaillard A, Ghiviriga I, Abboud KA, Murray LJ. *Inorg Chem.* 2014;53:4647–4654.
[16]Lane AC, Vollmer MV, Laber CH, Melgarejo DY, Chiarella GM, Fackler JP, Jr, Yang X, Baker GA, Walensky JR. *Inorg Chem*. 2014;53:11357–11366.
[17]Yang L, Powell DR, Houser RP. *Dalton Trans.* 2007:955.

[18]Xie X, Gorelsky SI, Sarangi R, Garner DK, Hwang HJ, Hodgson KO, Hedman B, Lu Y, Solomon EI. *J Am Chem Soc.* 2008;130:5194–5205.
[19]Li L, Murthy NN, Telser J, Zakharov LN, Yap GPA, Rheingold AL, Karlin KD, Rokita SE. *Inorg Chem.* 2006;45:7144–7159.
[20]Culpepper MA, Cutsail GE, III, Hoffman BM, Rosenzweig AC. *J Am Chem Soc.* 2012;134:7640–7643.
[21]Smith SM, Rawat S, Telser J, Hoffman BM, Stemmler TL, Rosenzweig AC. *Biochemistry*. 2011;50:10231–10240.
[22]Jiang X, Bollinger JC, Baik M-H, Lee D. *Chem Commun.* 2005;1043

Supplementary Material

Supporting Information

Contents:

EXPERIMENTAL

General Considerations. Unless otherwise specified, all reactions and manipulations were performed under purified N_2 in a glovebox or using standard Schlenk line techniques. Glassware was oven-dried prior to use. Reaction solvents (diethyl ether, toluene, tetrahydrofuran, dichloromethane, acetonitrile, pentane) were sparged with argon and dried using a Glass Contour Solvent System built by Pure Process Technology, LLC. Chloroform was degassed, dried and distilled. Unless otherwise specified, all chemicals were purchased from commercial sources and used without further purification.

Physical Measurements. NMR spectra for compound characterization were recorded at ambient temperatures using Bruker Avance DPX-400 or Bruker Avance DRX-500 MHz spectrometers. Low temperature NMR spectra were recorded on a Bruker Avance DRX-500 MHz spectrometer and low temperatures were attained from liquid nitrogen boiloff. Equations (1) and (2) were used to calculate magnetic moment (B.M.) and molar susceptibility, respectively, using Evans' Method.

$$\mu_{eff} = \sqrt{8\ x\ X_m\ x\ T\ (K)} \tag{1}$$

$$X_m = \frac{477\ x\ \Delta(Hz)}{2\ x\ Instrument\ frequency\ (Hz)\ x\ Molar\ concentration} \tag{2}$$

^{1}H and ^{13}C NMR chemical shifts were referenced to residual solvent peaks. FT-IR spectra were recorded on solid samples in a glovebox using a Bruker ALPHA spectrometer fitted with a diamond-ATR detection unit. Elemental analyses were performed by the Midwest Microlab, LLC in Indianapolis, IN. Deuterated solvents were degassed by repeated freeze-pump-thaw

cycles and then stored over 3-Å molecular sieves. UV-Vis absorbance spectra were taken at room temperature using a Cary 300 Bio UV-Visible Spectrophotometer.

Electrochemical data was measured at room temperature using a WaveNow USB Potentiostat from Pine Research Instrumentation. In a classic three-electrode system, a platinum working electrode, platinum counter electrode and a $Ag/AgNO_3$ (0.01 M $AgNO_3$/0.1M Bu_4NPF_6 in THF or dichloromethane) reference electrode was used. Compound **1** was dissolved in a 0.1 M solution of Bu_4NPF_6 in THF or dichloromethane at approximately 1 mM concentrations. Electrochemical measurements were referenced to approximately 1mM solutions of $FeCp_2^{+/0}$ in same electrolyte solution.

X-band EPR spectra at 110 K to 150 K were obtained with a Bruker EMX spectrometer located at the National Biomedical EPR Center at the Medical College of Wisconsin. Spectra were simulated (not shown) with EasySpin[1] (Stoll, S.; Schweiger, A.J.; J. Magn. Reson., 2006, 78,42). Samples of 5 mM **1** were glassed in toluene spiked with 3-5 drops of dichloromethane. The full spectrum of **1** shown in the main text utilized microwave frequency 9.297 GHz, temp 115 K, 9 scans, microwave power 5 mW, mod. Amp. 5G, mod. Freq. 100 kHz, time constant 81.92 ms, sweep time 83.886 s. The insert focusing on the $g_{\parallel}$ region utilized microwave frequency 9.277 GHz, 25 scans, time constant 81.92 ms, sweep time 42.943 s.

X-ray crystallography. X-ray crystallography data was collected at the X-ray Structural Laboratory at Marquette University (Milwaukee, WI). The X-ray single-crystal diffraction data were collected with an Oxford Diffraction SuperNova diffractometer equipped with dual microfocus Cu/Mo X-ray sources, X-ray mirror optics, Atlas CCD detector and low-temperature

---

([1]) Stoll, S.; Schweiger, A.J. *J. Magn. Reson.* **2006**, *78*, 42

Cryojet device. Data was collected using Cu(Kα) radiation at 100 K. The data was processed with CrysAlisPro program package (Oxford Diffraction Ltd., 2010) typically using a numerical Gaussian absorption correction (based on the real shape of the crystal) followed by an empirical multi-scan correction using SCALE3 ABSPACK routine. The structures were solved using SHELXS program and refined with SHELXL program[2] within Olex2 crystallographic package.[3] All computations were performed on an Intel PC computer under Windows 7 OS. The structure contained a certain degree of disorder, as described in the main text, which was detected in difference Fourier syntheses of electron density and was taken care of using capabilities of SHELX package (see Figure S15 and caption for more information). Hydrogen atoms were localized in difference syntheses of electron density but were refined using appropriate geometric restrictions on the corresponding bond lengths and bond angles within a riding/rotating model (torsion angles of Me hydrogens were optimized to better fit the residual electron density). A solvent-mask procedure was applied to account for additional electron density that could not be assigned definitively to a co-crystallized solvent.

Preparation of Bis(2,4,6-trimethylphenyl)formamidine. A literature procedure was followed for the isolation of bis(2,4,6-trimethylphenyl)formamidine.[4] This synthesis took place in open air and acetone was used as the recrystallization solvent.

---

(2) Sheldrick, G. M. *Acta Cryst*. **2008**, *A64*, 112–122.

(3) Dolomanov, O. V.; Bourhis, L. J.; Gildea, R. J.; Howard, J. A. K.; Puschmann, H. *J. Appl. Cryst*. **2009**, *42*, 339–341.

(4) Kolychev, E. L.; Portnyagin, I. A. ; Shuntikov, V. V.; Khrustalev, V. N.; Nechaev, M.S. *J. Organomet. Chem*. **2009,** *694,* 2454.

Preparation of $Cu_2[(2,4,6\text{-}Me_3C_6H_2N)_2C(H)]_2$. A modified version of the reported literature procedure for $Cu_2[(2,6\text{-}Me_2C_6H_3N)_2C(H)]_2$[5] was used as follows. Bis(2,4,6-trimethylphenyl)formamidine (1.83 g, 6.53 mmol) was dissolved in THF (approximately 120 mL). Sodium bis(trimethylsilyl)amide (1.34 g, 7.31mmol) was added to the stirring THF solution at room temperature, and the yellow solution was stirred for 1 h. Tetrakis(acetonitrile)copper(I) hexafluorophosphate (2.43 g, 6.52 mmol) was added to the stirring solution, which became instantly cloudy white. Stirring was continued at room temperature overnight. The solution volume was completely evaporated by vacuum. The evaporated residue was reconstituted in dichloromethane and filtered through Celite to remove insoluble $NaPF_6$. The resulting yellow filtrate was vacuum evaporated until a precipitate formed. This solid was collected by filtration and washed with diethyl ether (2 x 5 mL). The resulting white solid was dried under vacuum, and the filtrate was further vacuum evaporated to collect multiple crops. Yield of $Cu_2[(2,4,6\text{-}Me_3C_6H_2N)_2C(H)]_2$: 93%. ^{1}H NMR (400 MHz, $CDCl_3$): δ 2.21 (s, 12H, *p*-CH_3), 2.30 (s, 24H, *o*-CH_3), 6.79 (s, 8H, Ar C-H), 6.98 (s, 2H, NCH). $^{13}C\{^1H\}$ NMR (100 MHz, $CDCl_3$): δ 169.8 (NC(H)N), 144.4 (quat C, Ar), 133.4 (quat *p*-C, Ar), 132.8 (quat *o*-C, Ar), 128.7 (*m*-CH, Ar), 20.6 (Ar *p*-CH_3), 19.3 (Ar *o*-CH_3). FT-IR (cm^{-1}): 3002, 2903, 2848, 1611 (N=C), 1567, 1474, 1429, 1372, 1334, 1231, 1210, 1146, 1007, 846, 624, 583, 513, 418.

Preparation of $[Cu_4(\mu_4\text{-}S)(\mu_2\text{-}NCN)_4]$ (1) using S_8. $Cu_2[(2,4,6\text{-}Me_3C_6H_2N)_2C(H)]_2$ (0.300 g, 0.437 mmol) was dissolved in minimum amount of THF (~ 3 mL) using a magnetic stir bar. In a separate vessel, S_8 (0.007 g, 0.027 mmol) was stirred in 0.5 mL toluene until completely dissolved. The toluene solution of S_8 was then added to the $Cu_2[(2,4,6\text{-}Me_3C_6H_2N)_2C(H)]_2$

([5]) Lane, A. C.; Vollmer, M. V.; Laber, C. H.; Melgarejo, D. Y.; Chiarella, G. M.; Fackler Jr., J. P.; Yang, X.; Baker, G. A.; Walensky, J. R. *Inorg. Chem.* **2014,** *53,* 11357.

solution dropwise, with stirring, at room temperature. Once all the S_8 solution had been added, the color began to change steadily to purple. The solution was stirred vigorously at 40-43° C overnight. The next day the solution was black. The solution was completely evaporated by vacuum. To the evaporated residue was added a small amount (~ 1 mL) of dichloromethane to make a super-saturated solution and was filtered. The dark solid was then washed with dichloromethane (2 x 4 mL) to remove unreacted $Cu_2[(2,4,6\text{-}Me_3C_6H_2N)_2C(H)]_2$, then diethyl ether (approximately 10 mL) to remove any remaining dichloromethane solvent, and finally acetonitrile (approximately 10 mL or until filtrate is clear) to remove a red-colored side product. Using a new, clean vacuum flask, the purple solid was extracted with copious amounts of dichloromethane until filtrate appeared clear. The purple filtrate was then pipette-filtered through Celite, and the solution was then completely evaporated under vacuum – after the filtrate is pipette-filtered through Celite, it should be evaporated as soon as possible to avoid decomposition into $Cu_2[(2,4,6\text{-}Me_3C_6H_2N)_2C(H)]_2$. Yield of **1**: 0.107 g, 34%. Compound **1** was stored in a freezer (-36°C) and is not stable in solution at room temperature for long periods of time. Note: Trace amounts (5-10%) of the starting material, ($Cu_2[(2,4,6\text{-}Me_3C_6H_2N)_2C(H)]_2$), were often detected by ^{1}H NMR regardless of multiple purification attempts. A good method for removing $Cu_2[(2,4,6\text{-}Me_3C_6H_2N)_2C(H)]_2$ is by adding a small amount of dichloromethane to the solid so that $Cu_2[(2,4,6\text{-}Me_3C_6H_2N)_2C(H)]_2$ dissolves but **1** is super-saturated and doesn't entirely dissolve. This solution is filtered, and the purple solid is washed with a small amount of dichloromethane and then diethyl ether to remove dichloromethane solvent. The purple solid can then be collected and dried under vacuum. Usually this purification method is done twice to achieve analytical purity. Dark black crystals may be obtained by dissolving purple **1** in a minimum amount of chloroform and allowing pentane vapors to diffuse in through a pin sized

hole. ^{1}H NMR (400 MHz, $CDCl_3$): δ 1.30 (s, 12 H, CH_3), 1.38 (s, 12 H, CH_3), 2.16 (s, 12 H, CH_3), 2.18 (s, 12 H, CH_3), 2.68 (s, 12 H, CH_3), 2.75 (s, 12 H, CH_3), 6.12 (s, 2 H, NC(H)N), 6.24 (s, 4 H, Ar CH), 6.30 (s, 4 H, Ar CH), 6.65 (s, 2 H, NC(H)N), 6.70 (s, 8 H, Ar CH). ^{13}C{^{1}H} NMR (100 MHz, $CDCl_3$): δ 172 (NC(H)N), 160 (NC(H)N), 144.5 (Ar), 144.3 (Ar), 133.6 (Ar), 133.4 (Ar), 132.7 (Ar), 132.58 (Ar), 132.53 (Ar), 128.7 (Ar), 128.5 (Ar), 128.2 (Ar), 128.0 (Ar), 21 (Ar *p*-CH_3), 20.7 (Ar *p*-CH_3), 20.4 (Ar *o*-CH_3), 18 (Ar *o*-CH_3), 17 (Ar *o*-CH_3). FT-IR (cm^{-1}): 2981, 2912, 2851, 1610 (N=C), 1553, 1530, 1471, 1372, 1339, 1325, 1224, 1206, 1144, 1029, 850, 735, 588, 571, 505, 460, 442, 412. Anal. calcd. for $C_{76}H_{92}Cu_4N_8S$: C, 65.0; H, 6.61; N, 7.98. Found: C, 64.91; H, 6.60; N, 8.06.

Preparation of [Cu_4(μ_4-S)(μ_2-NCN)$_4$] (1) using Ph_3SbS. $Cu_2[(2,4,6\text{-}Me_3C_6H_2N)_2C(H)]_2$ (0.258 g, 0.376 mmol) was dissolved in minimum amount of THF (~ 3 mL) using a magnetic stir bar. In a separate vessel, Ph_3SbS (0.0727 g, 0.188 mmol) was dissolved in 2 mL THF. The solution of Ph_3SbS solution was then added to the $Cu_2[(2,4,6\text{-}Me_3C_6H_2N)_2C(H)]_2$ solution dropwise, with stirring, at room temperature. Once all the Ph_3SbS solution had been added, the color rapidly began to change from yellow to orange then maroon. The solution was stirred vigorously at room temperature overnight. The next day the solution was black. The solution was completely evaporated by vacuum. To the evaporated residue was added a small amount (~ 1 mL) of dichloromethane to make a super-saturated solution, which was filtered through Celite. The dark solid on the Celite pad was then washed with dichloromethane (2 x 6 mL) to remove unreacted $Cu_2[(2,4,6\text{-}Me_3C_6H_2N)_2C(H)]_2$, then diethyl ether (approximately 6 mL) to remove any remaining dichloromethane solvent, and finally acetonitrile (approximately 10 mL or until filtrate is clear) to remove any remaining triphenyl-antimony containing byproducts (usually appearing in ^{1}H NMR at δ 7.24- 7.15 ppm in $CDCl_3$). Using a new, clean vacuum flask, the

purple solid remaining on the Celite was collected with copious amounts of dichloromethane until the filtrate became clear (~ 100 mL). The dark purple filtrate was completely evaporated by vacuum. This filtrate should be evaporated as soon as possible to avoid decomposition into $Cu_2[(2,4,6\text{-}Me_3C_6H_2N)_2C(H)]_2$. Yield of **1**: 0.1144 g, 43%. Note: Trace amounts (5-10%) of the starting material, ($Cu_2[(2,4,6\text{-}Me_3C_6H_2N)_2C(H)]_2$), were often detected by ^1H NMR regardless of multiple purification attempts. The best method for removing $Cu_2[(2,4,6\text{-}Me_3C_6H_2N)_2C(H)]_2$ is by adding a small amount of dichloromethane to the solid so that $Cu_2[(2,4,6\text{-}Me_3C_6H_2N)_2C(H)]_2$ dissolves but **1** is super-saturated and doesn't entirely dissolve. This saturated solution is filtered, and the purple solid is washed with a small amount of dichloromethane and then diethyl ether to remove dichloromethane solvent. The purple solid can then be collected and dried under vacuum. Dark black crystals may be obtained by dissolving purple **1** in a minimum amount of chloroform and allowing pentane vapors to diffuse in through a pin sized hole.

Experimental Conditions: Low temperature NMR Evans' Method of **1**

$Cu_4S(NCN)_4$ (0.0015 g, 0.0010 mmol) was dissolved in $CDCl_3$ and 100 µL of $CHCl_3$ was added. Total weight of solution was 1.7571 g. The solution was then pipette-filtered through Celite into an NMR tube. A glass capillary tube (approximately 17 cm in length and approximately 3 mm in diameter) was syringe filled with $CHCl_3$ and then inserted into the NMR tube containing the $Cu_4S(NCN)_4$ solution. The difference in chloroform peak chemical shifts were analyzed to determine magnetic moment using Evans' Method.

Table S1: Data used in calculating magnetic moment and molar susceptibility of **1** for low temperature NMR Evans' Method.

Temperature (K)	Peak 1 (ppm)	Peak 2 (ppm)
298	7.272	7.259
280	7.274	7.261
261	7.275	7.262
240	7.275	7.262
221	7.274	7.262

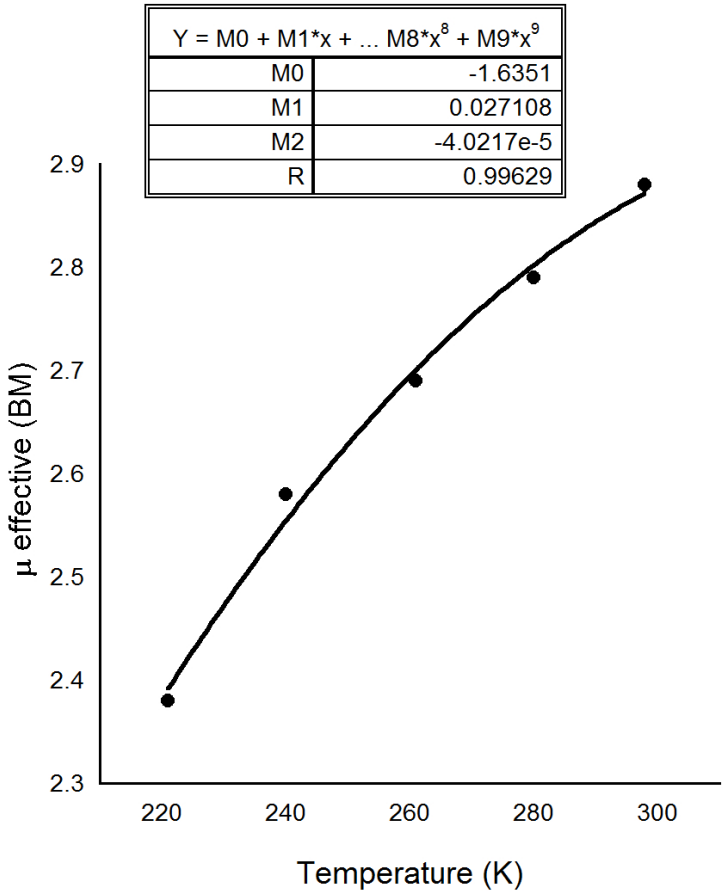

Figure S1: Change in magnetic moment of **1** depending on temperature studied by ^{1}H NMR Evans' Method analysis.

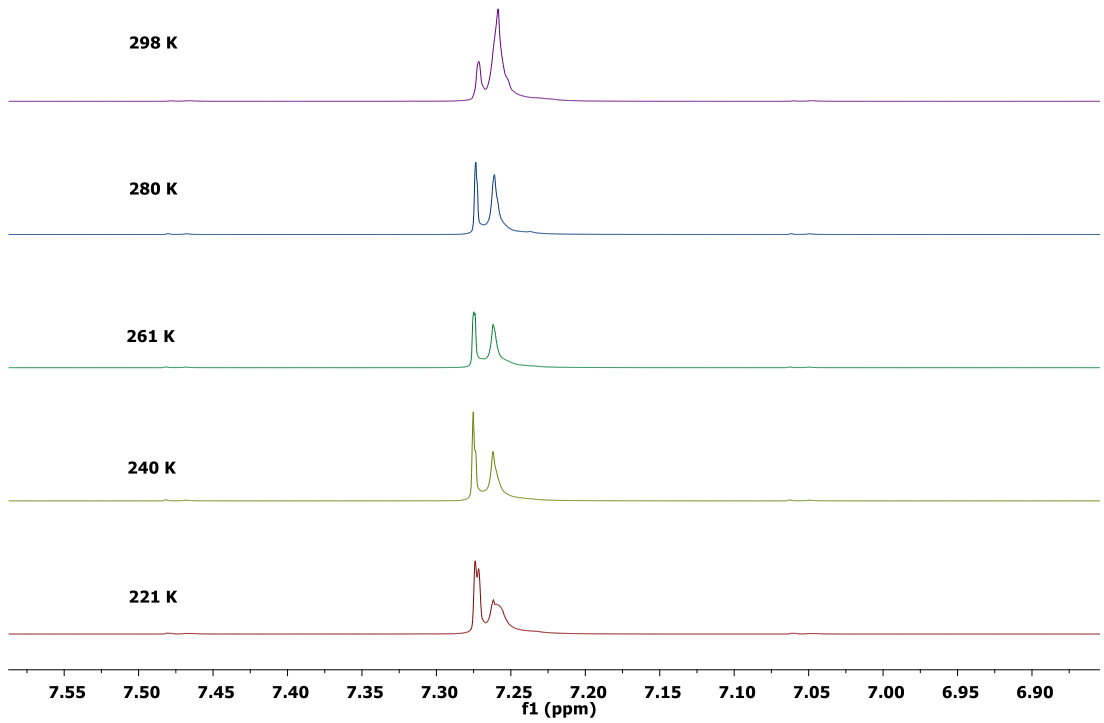

Figure S2: ^{1}H NMR (500 MHz) of **1** at different temperatures for Evans' Method analysis.

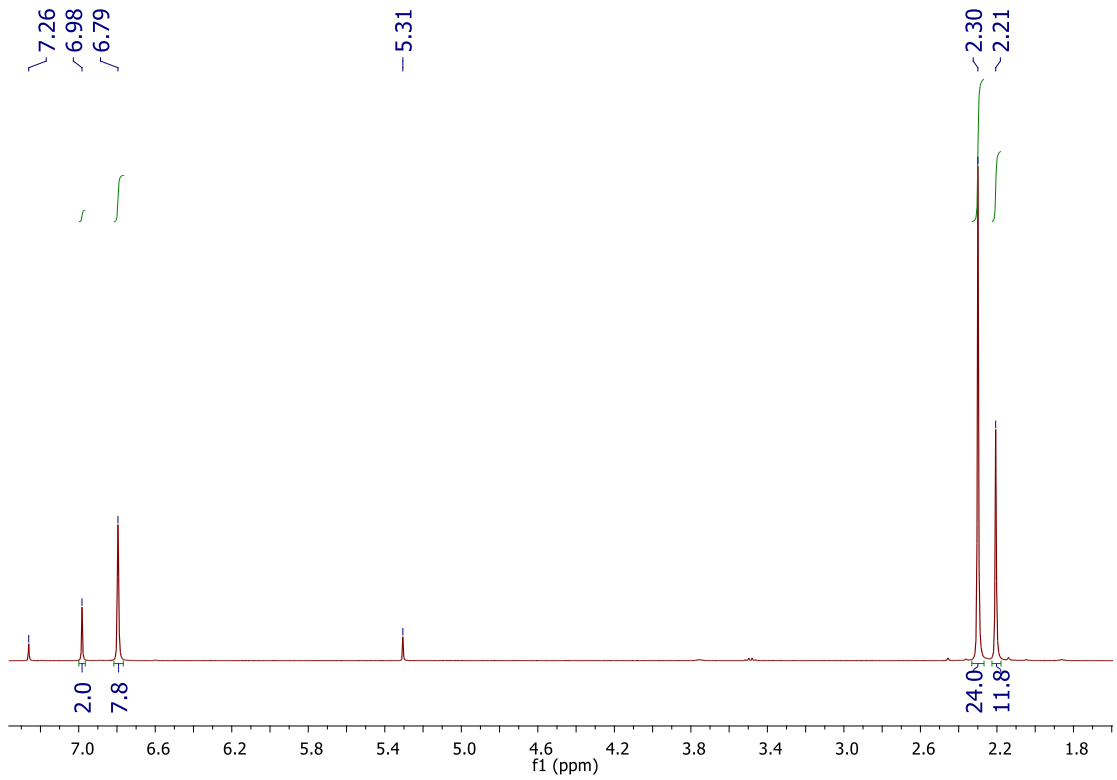

Figure S3. ^{1}H NMR (400 MHz) of $Cu_2[(2,4,6\text{-}Me_3C_6H_2N)_2C(H)]_2$ in $CDCl_3$. Peak observed at 5.31 ppm is residual dichloromethane.

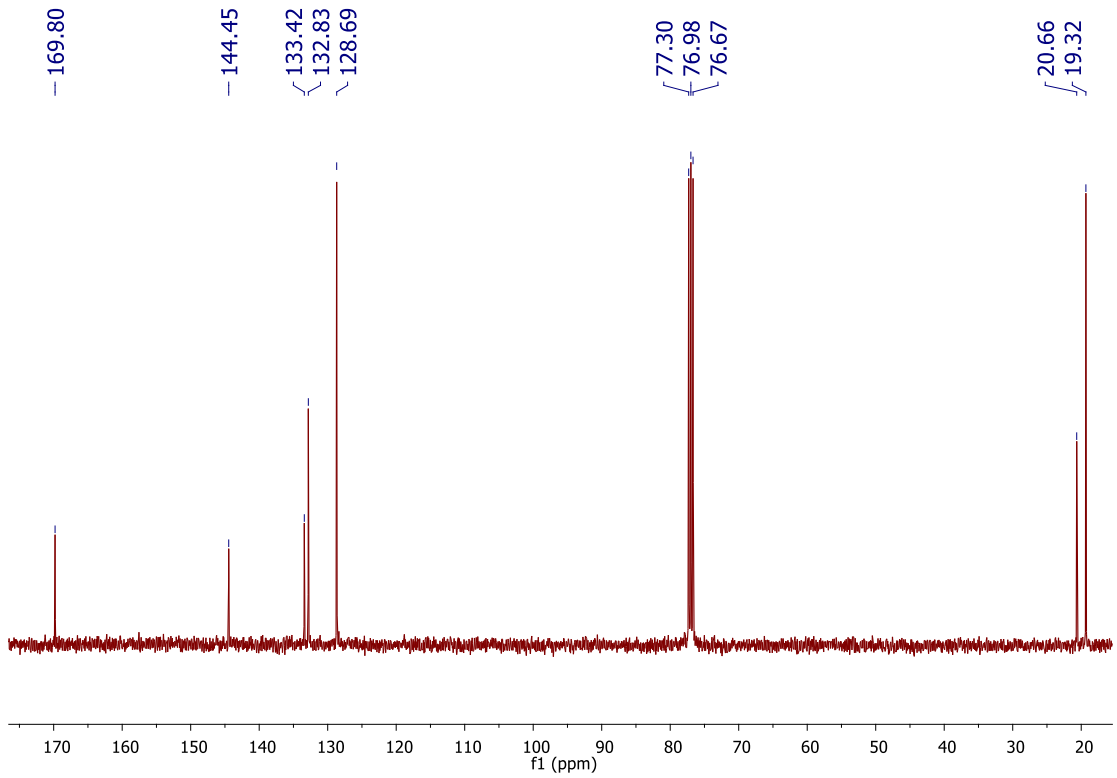

Figure S4. $^{13}C\{^{1}H\}$ NMR (100 MHz) of $Cu_2[(2,4,6\text{-}Me_3C_6H_2N)_2C(H)]_2$ in $CDCl_3$.

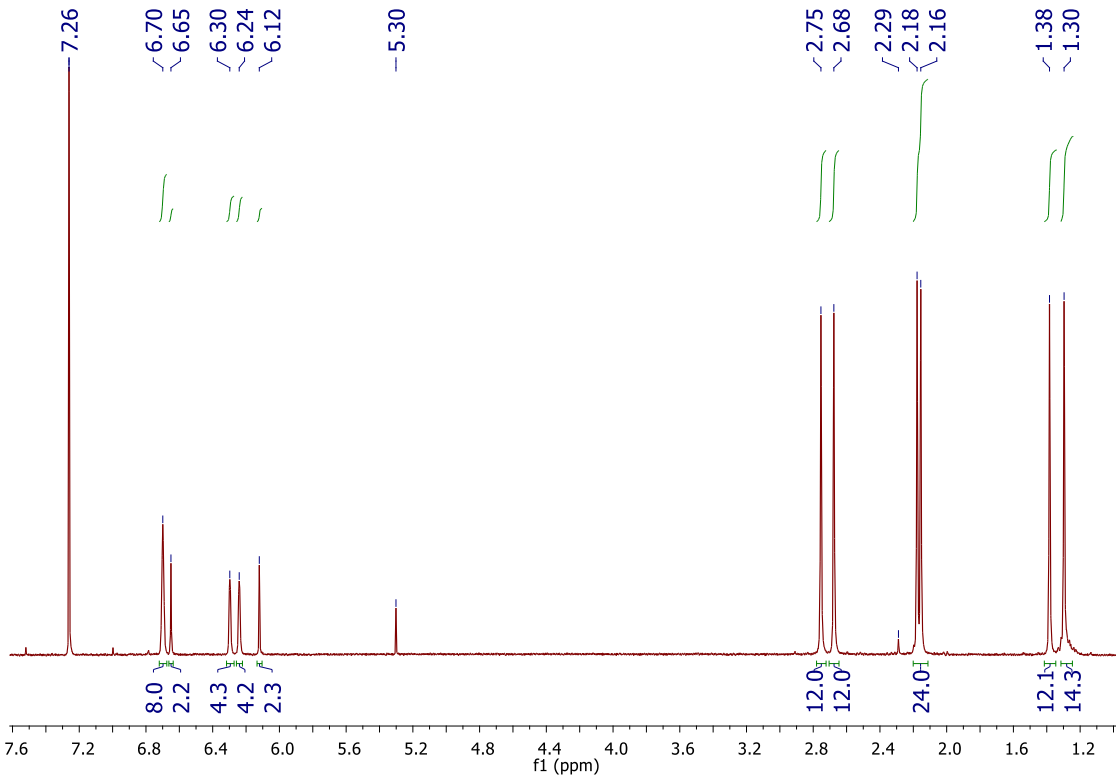

Figure S5: ^{1}H NMR (400 MHz) of **1** in $CDCl_3$. Peak observed at 5.30 ppm is residual dichloromethane. Peak observed at 2.29 ppm is trace amount of $Cu_2[(2,4,6\text{-}Me_3C_6H_2N)_2C(H)]_2$.

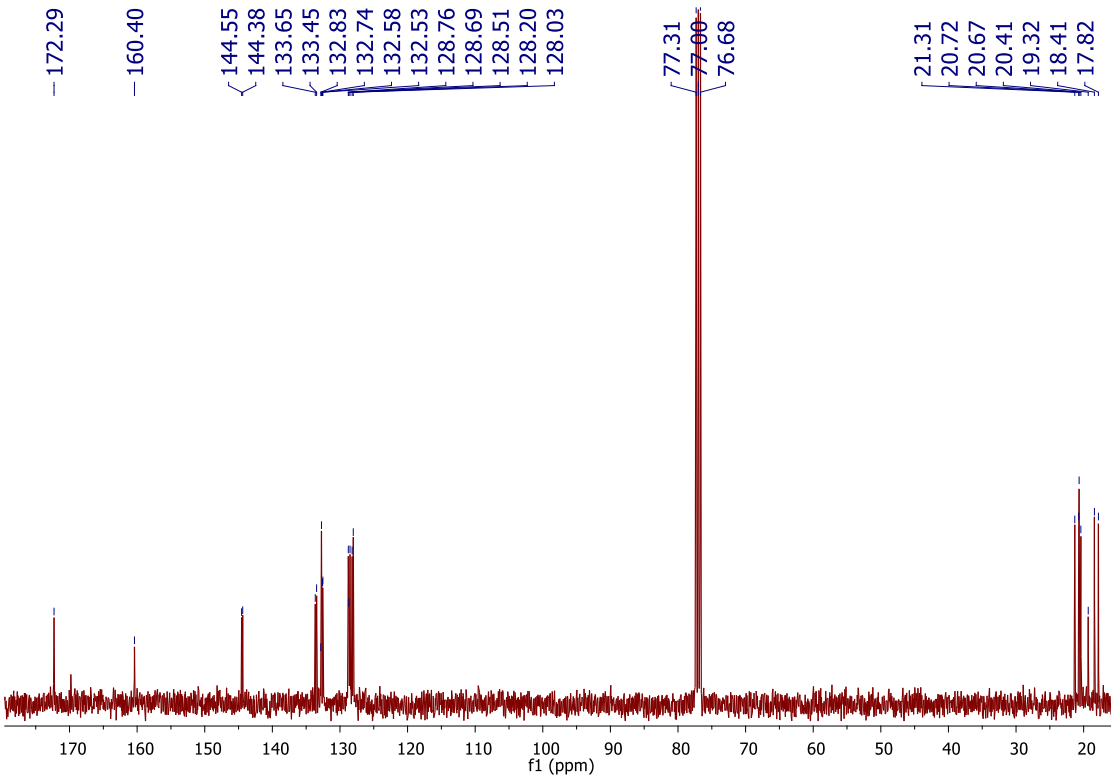

Figure S6: ^{13}C NMR (100 MHz) of **1** in $CDCl_3$. Peak observed at the following chemical shifts are residual amounts of $Cu_2[(2,4,6\text{-}Me_3C_6H_2N)_2C(H)]_2$; 132.8 ppm, 128.69 ppm, 20.67 ppm and 19.3 ppm.

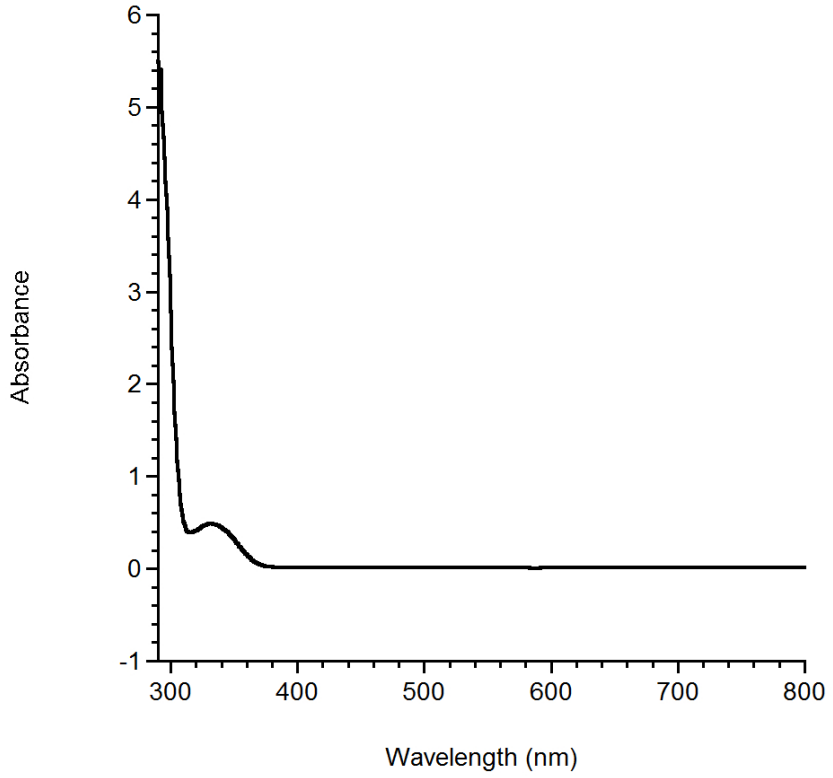

Figure S7: Absorption Spectra for 0.3 mM $Cu_2[(2,4,6\text{-}Me_3C_6H_2N)_2C(H)]_2$ in dichloromethane.

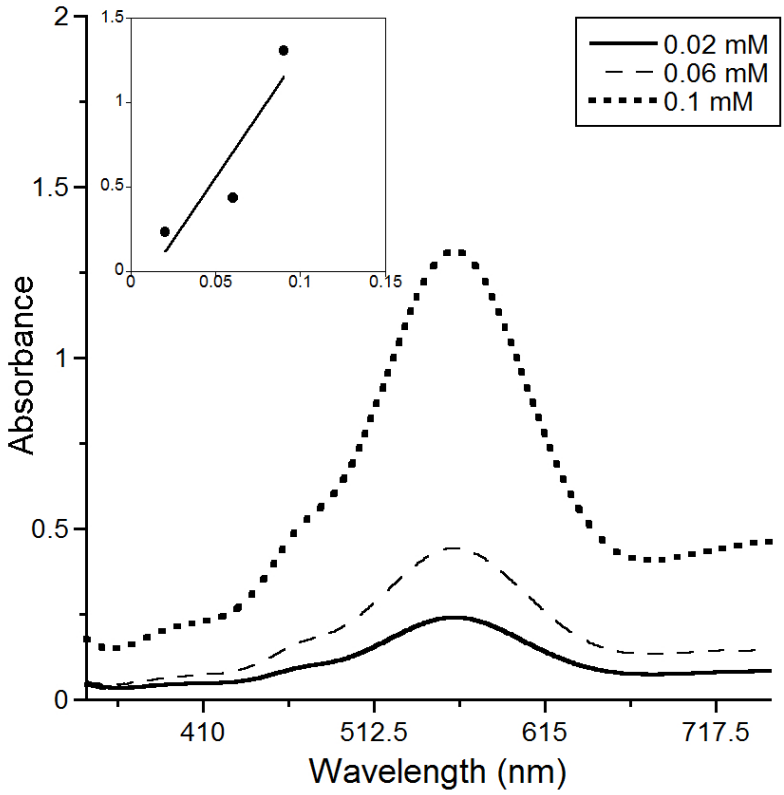

Figure S8: Absorption Spectra for **1** in dichloromethane at different concentrations. Inset plot of absorbance vs. concentration (mM); ε = 14000 M^{-1}•cm^{-1} (y = -0.1712 + 14.746x; R= 0.9100).

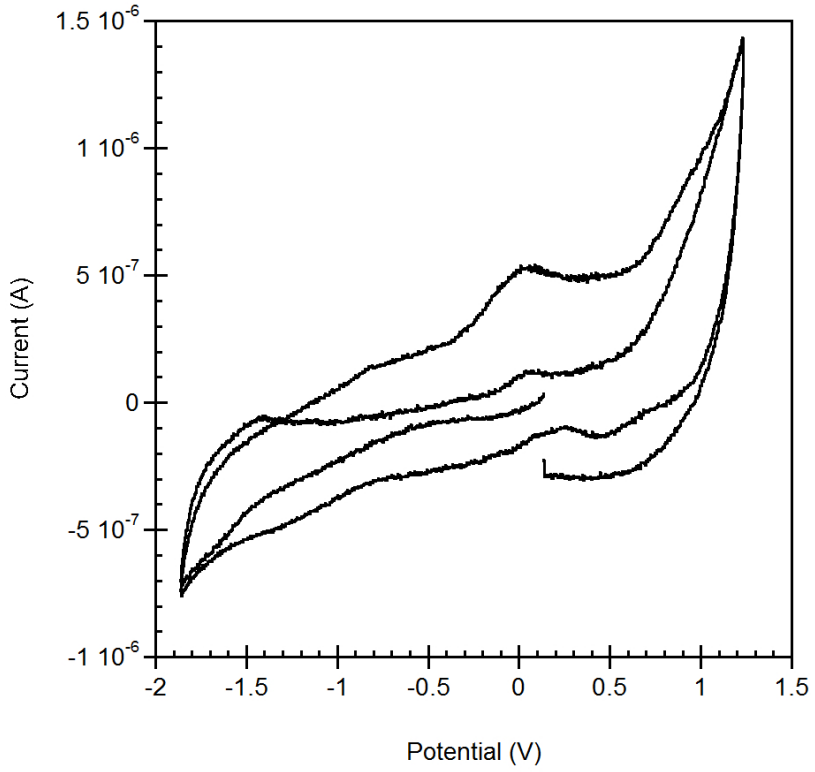

Figure S9: Cyclic Voltammogram of 0.1 M Bu_4NPF_6 background in dichloromethane vs $FeCp_2^{+/0}$.

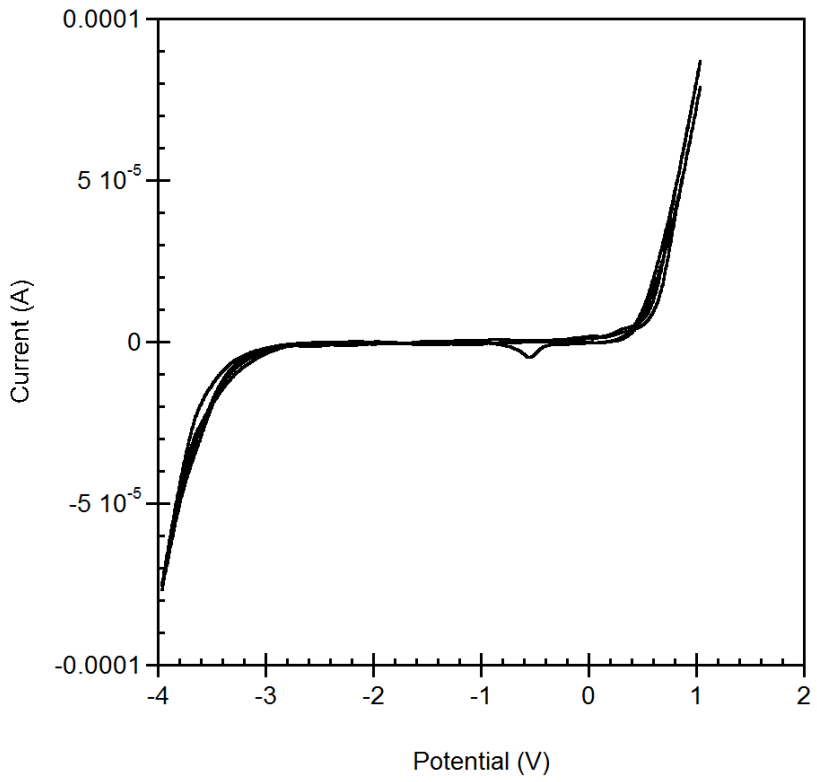

Figure S10: Cyclic Voltammogram of 0.1 M Bu_4NPF_6 background in THF vs. $FeCp_2^{+/0}$.

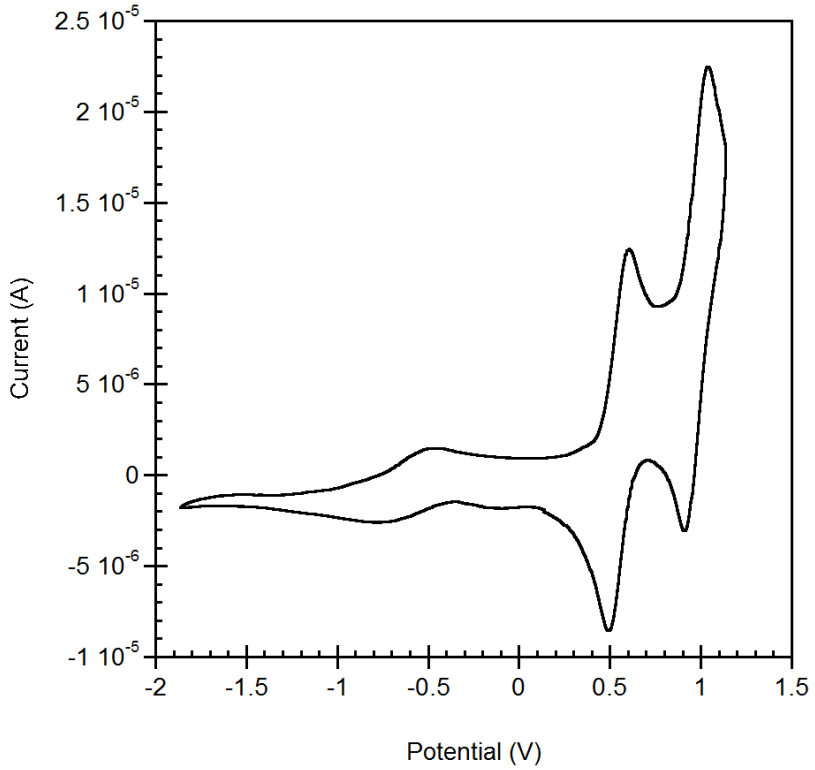

Figure S11: Cyclic Voltammogram of 1.48 mM $Cu_2[(2,4,6\text{-}Me_3C_6H_2N)_2C(H)]_2$ in dichloromethane vs. $FeCp_2^{+/0}$.

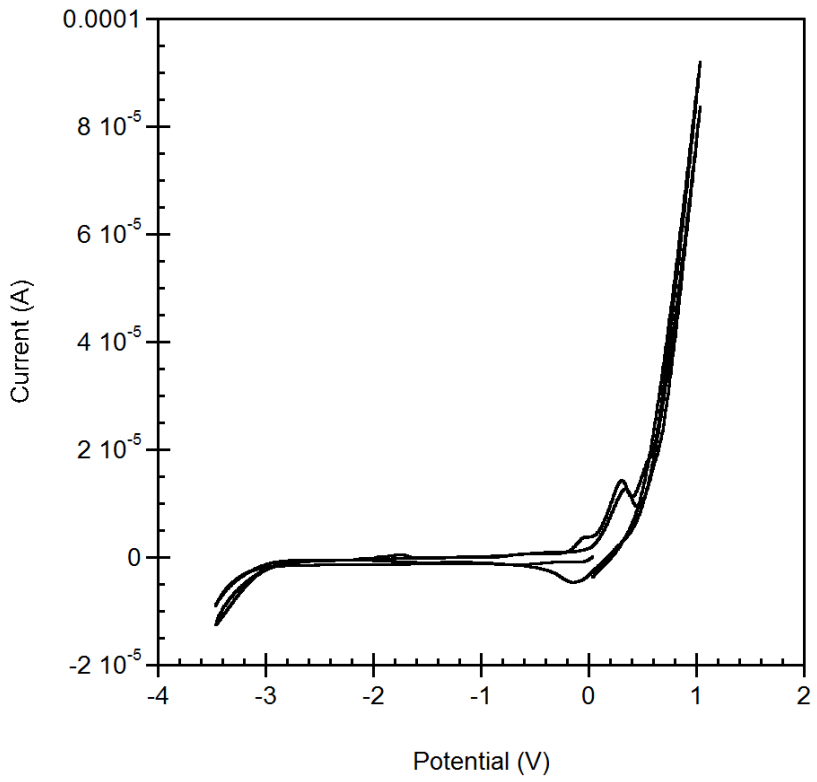

Figure S12: Cyclic Voltammogram of 0.63 mM $Cu_2[(2,4,6\text{-}Me_3C_6H_2N)_2C(H)]_2$ in THF vs. $FeCp_2^{+/0}$.

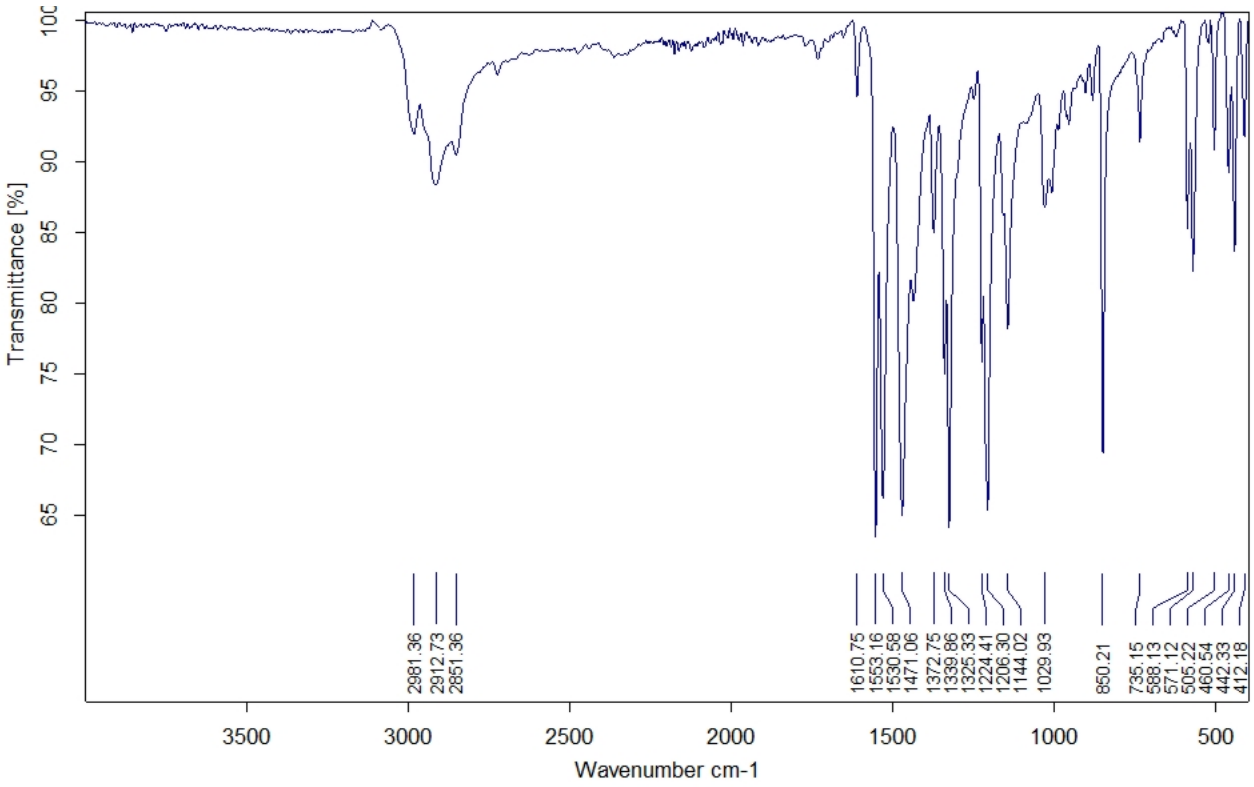

Figure S13: Infrared Spectrum of **1**.

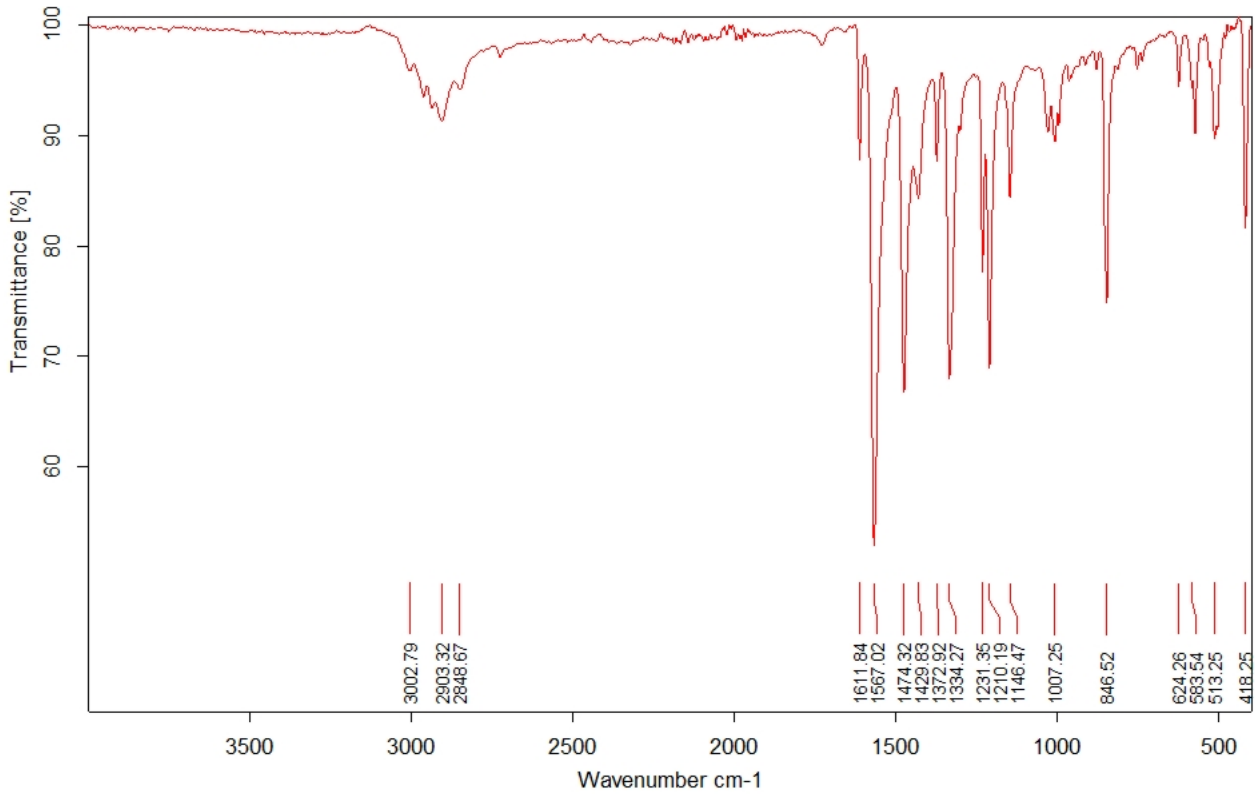

Figure S14: Infrared Spectrum of $Cu_2[(2,4,6\text{-}Me_3C_6H_2N)_2C(H)]_2$.

COMPUTATIONAL METHODS

All calculations were performed using Gaussian09, Revision B.01.[6] Density functional theory (DFT) calculations were carried out using a hybrid functional, BVP86, consisting of Becke's 1988 gradient-corrected Slater exchange functional[7] combined with the VWNS local electron correlation functional and Perdew's 1986 nonlocal electron correlation functional.[8] Mixed basis sets were employed: the LANL2TZ(f) triple-ζ basis set[9] with effective core potential[10] was used for Cu, the Gaussian09 internal 6-311+G(d) basis set was used for S, and the Gaussian09 internal 6-31+G(d) basis set was used for C, H, and N. The crystal structure of **1** was used as a starting point for constructing the input file: the mesityl groups were changed to methyl groups, and only one set of Cu_4S coordinates were used. All calculations were spin-unrestricted and symmetry-unrestricted. Final output wavefunctions were tested for stability against antiferromagnetic coupling (see: http://www.gaussian.com/g_tech/afc.htm) and were found to be stable. Orbital surfaces were analyzed using Gaussview, and orbital populations were determined using the Pop=Orbitals keyword in Gaussian09. Optimized coordinates for the singlet state of **1-Me** are enclosed below.

---

[6] Frisch, M. J.; Trucks, G. W.; Schlegel, H. B.; Scuseria, G. E.; Robb, M. A.; Cheeseman, J. R.; Scalmani, G.; Barone, V.; Mennucci, B.; Petersson, G. A.; Nakatsuji, H.; Caricato, M.; Li, X.; Hratchian, H. P.; Izmaylov, A. F.; Bloino, J.; Zheng, G.; Sonnenberg, J. L.; Hada, M.; Ehara, M.; Toyota, K.; Fukuda, R.; Hasegawa, J.; Ishida, M.; Nakajima, T.; Honda, Y.; Kitao, O.; Nakai, H.; Vreven, T.; Montgomery, J. A., Jr., Peralta, J. E.; Ogliaro, F.; Bearpark, M.; Heyd, J. J.; Brothers, E.; Kudin, K. N.; Staroverov, V. N.; Keith, T.; Kobayashi, R.; Normand, J.; Raghavachari, K.; Rendell, A.; Burant, J. C.; Iyengar, S. S.; Tomasi, J.; Cossi, M.; Rega, N.; Millam, J. M.; Klene, M.; Knox, J. E.; Cross, J. B.; Bakken, V.; Adamo, C.; Jaramillo, J.; Gomperts, R.; Stratmann, R. E.; Yazyev, O.; Austin, A. J.; Cammi, R.; Pomelli, C.; Ochterski, J. W.; Martin, R. L.; Morokuma, K.; Zakrzewski, V. G.; Voth, G. A.; Salvador, P.; Dannenberg, J. J.; Dapprich, S.; Daniels, A. D.; Farkas, O.; Foresman, J. B.; Ortiz, J. V.; Cioslowski, J.; , Fox, D. J. *Gaussian 09, Revision B.01; Gaussian*, Inc., Wallingford, CT, 2010.

[7] Becke, A. D. *Phys. Rev. A* **1988**, 38, 3098–100.

[8] Perdew, J. P. *Phys. Rev. B* **1986**, 33, 8822–24

[9] (a) Hay, P. J.; Wadt, W. R. *J. Chem. Phys.* **1985**, 82, 299. (b) Roy, L. E.; Hay, P. J.; Martin, R. L. *J. Chem. Theory Comput.* **2008**, 4, 1029. (c) Ehlers, A. W.; Bohme, M.; Dapprich, S.; Gobbi, A.; Hollwarth, A.; Jonas, V.; Kohler, K. F.; Stegmann, R.; Veldkamp, A.; Frenking, G. *Chem. Phys. Lett.* **1993**, 208, 111.

[10] (a) Hay, P. J.; Wadt, W. R. *J. Chem. Phys.* **1985**, 82, 270. (b) Hay, P. J.; Wadt, W. R. *J. Chem. Phys.* **1985**, 82, 284. (c) Hay, P. J.; Wadt, W. R. *J. Chem. Phys.* **1985**, 82, 299.

Cu1 Cu -1.3232 1.3228 -0.2204

S2 S 9.01401e-17 -0.0001 -1.472

Cu7 Cu 1.3231 -1.3227 -0.2202

Cu12 Cu 1.1189 1.4595 -0.15

N13 N 0.951 2.6674 1.375

N14 N -1.4014 2.5711 1.2715

C15 C -0.2624 2.9922 1.8152

H16 H -0.3289 3.6517 2.706

Cu17 Cu -1.1189 -1.4595 -0.1498

N18 N -0.9509 -2.6671 1.3754

N19 N 1.4016 -2.5707 1.2719

C20 C 0.2626 -2.992 1.8156

H21 H 0.3291 -3.6515 2.7063

C30 C 2.1006 3.2074 2.094

H31 H 2.8286 2.4073 2.3177

H32 H 2.6238 3.98 1.4974

H33 H 1.7988 3.6724 3.0545

C34 C -2.654 3.0268 1.8641

H35 H -3.345 2.1765 2.0013

H36 H -2.4893 3.5005 2.8533

H37 H -3.1614 3.7695 1.2166

C46 C -2.1005 -3.2072 2.0944

H47 H -1.7986 -3.6726 3.0547

H48 H -2.8283 -2.407 2.3185

H49 H -2.624 -3.9794 1.4976

C50 C 2.6542 -3.0266 1.8644

H51 H 2.4896 -3.5002 2.8536

H52 H 3.1615 -3.7693 1.2168

H53 H 3.3453 -2.1763 2.0014

N3 N -3.1307 0.9736 -0.9666

N4 N -2.9782 -1.3951 -0.8587

C5 C -3.5863 -0.257 -1.1737

H6 H -4.5845 -0.3419 -1.6504

C38 C -3.9049 2.0935 -1.4931

H39 H -4.8927 1.7673 -1.8774

H40 H -4.082 2.8517 -0.7085

H41 H -3.3694 2.5931 -2.3242

C42 C -3.6538 -2.647 -1.1882

H43 H -3.8477 -3.2471 -0.2795

H44 H -4.6269 -2.4703 -1.6895

H45 H -3.0327 -3.2617 -1.867

N8 N 3.1306 -0.9739 -0.9666

N9 N 2.9783 1.3948 -0.8589

C10 C 3.5862 0.2567 -1.1738

H11 H 4.5844 0.3415 -1.6506

C22 C 3.9042 -2.0938 -1.494

H23 H 4.0794 -2.8534 -0.7103

H24 H 3.3694 -2.5915 -2.3266

H25 H 4.893 -1.7681 -1.8762

C26 C 3.6542 2.6467 -1.1877

H27 H 4.6266 2.4699 -1.6904

H28 H 3.0326 3.2625 -1.865

H29 H 3.8496 3.2457 -0.2786

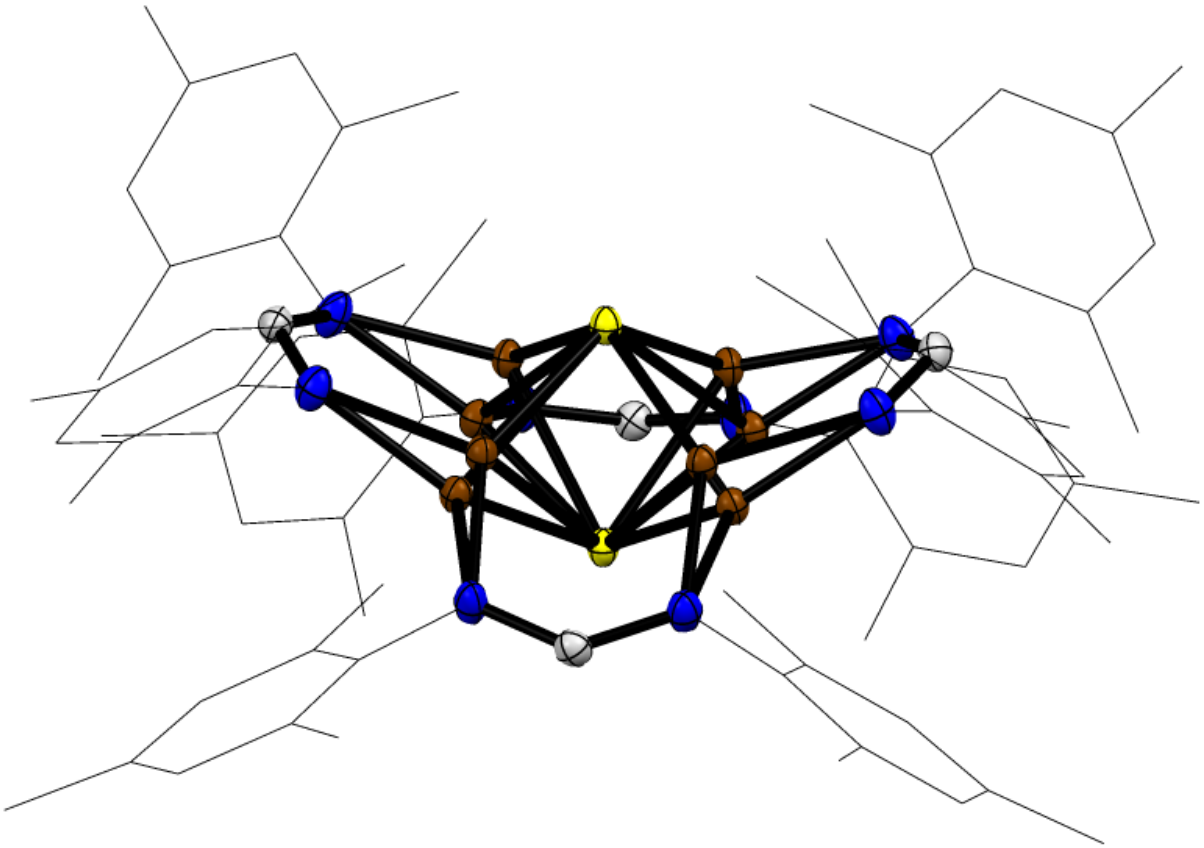

Figure S15. Solid-state structure of **1** determined by X-ray crystallography, with both disordered Cu_4S components shown. The molecule is positioned on crystallographic element of symmetry (-4) and experiences two types of disorder: (a) the S cap alternatively occupies 2 symmetrically equivalent position over and under the Cu_4 moiety, and (b) each of the Cu ions of the central moiety deviates alternatively up or down from the mean plane that corresponds to a superposition of two tetrahedral distortions of opposite sign. The ligands do not show any perceptible disorder. Apparently, they form a significantly robust scaffold around the central metal nucleus owing to stacking between their overlapping mesityl groups.

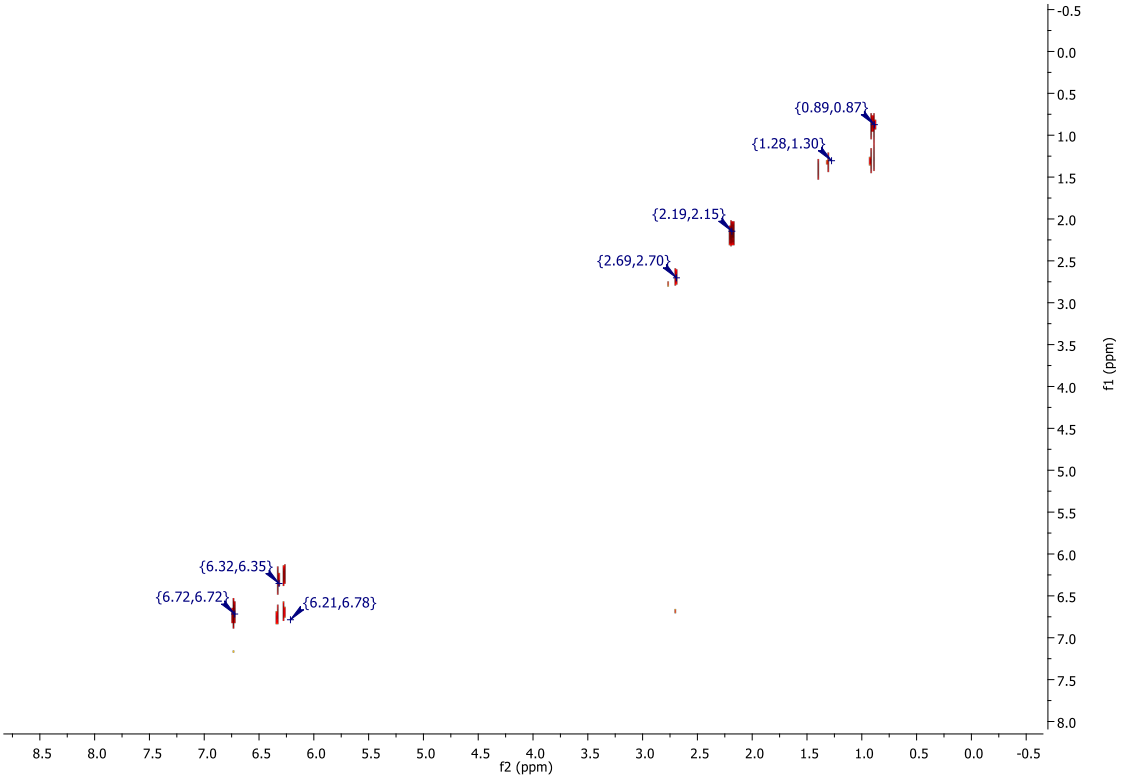

Figure S16: ^{1}H-^{1}H COSY (500 MHz) of **1** in $CDCl_3$, showing that none of the signals observed by ^{1}H NMR are coupled to one another. Correlation seen at 0.89 ppm is residual pentane solvent.

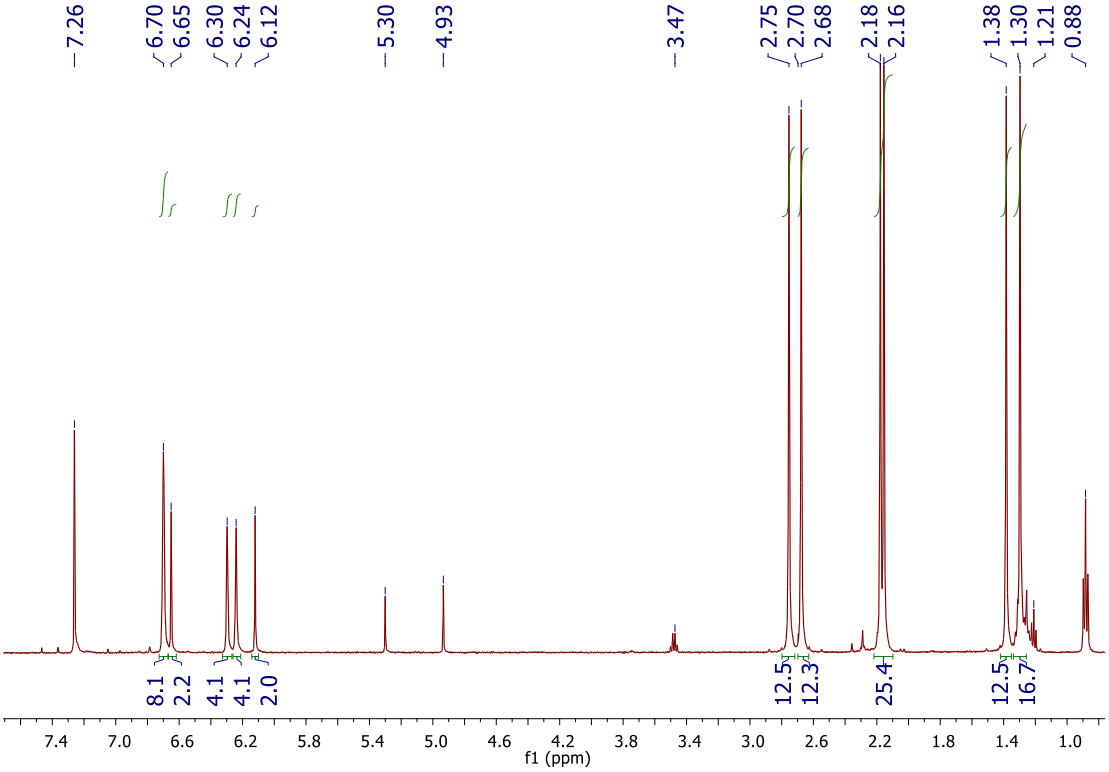

Figure S17: ^{1}H NMR (500 MHz) of **1** in $CDCl_3$ sample used for ^{1}H-^{1}H COSY experiment in Figure S16. Peaks observed at the following chemical shifts are residual solvents in sample: 0.88 ppm (pentane), 1.21 ppm and 3.47 ppm (diethyl ether), 4.93 ppm (dibromomethane), 5.30 ppm (dichloromethane).

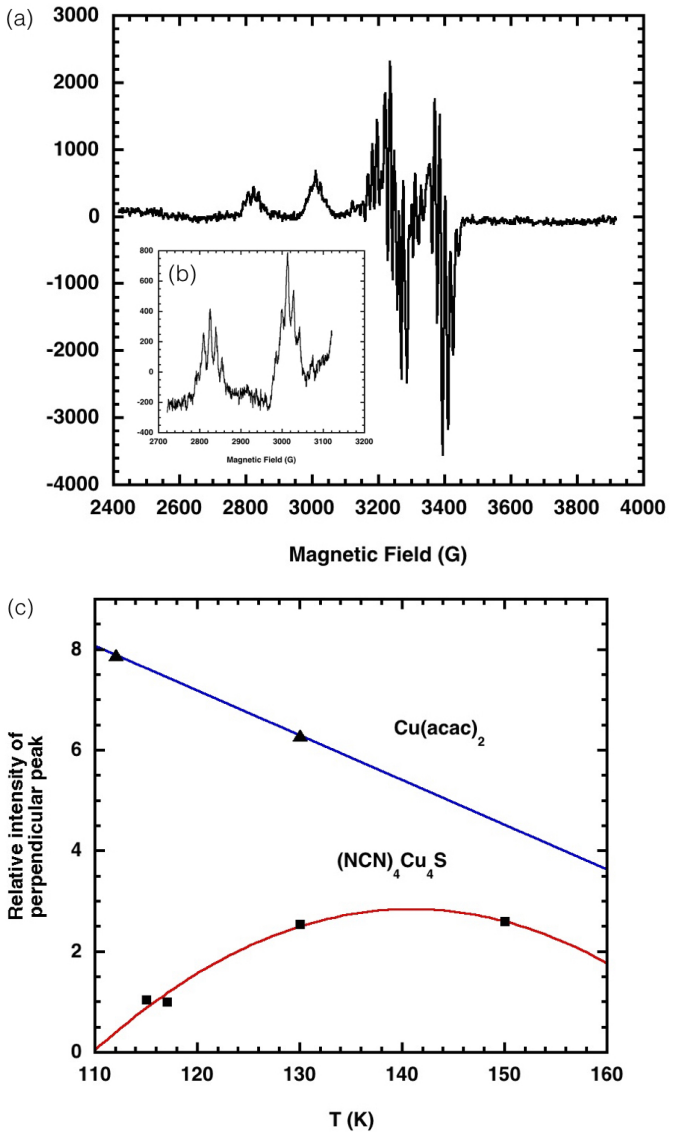

Figure S18. (a) X-band EPR spectrum of **1** in toluene glass at 115 K; (b) the $g_{\parallel}$ region of the EPR spectrum; (c) temperature dependence of EPR signal intensity for **1** and for a $Cu(acac)_2$ control, with curves drawn to guide the eye.